Nanoscale

Accepted Manuscript

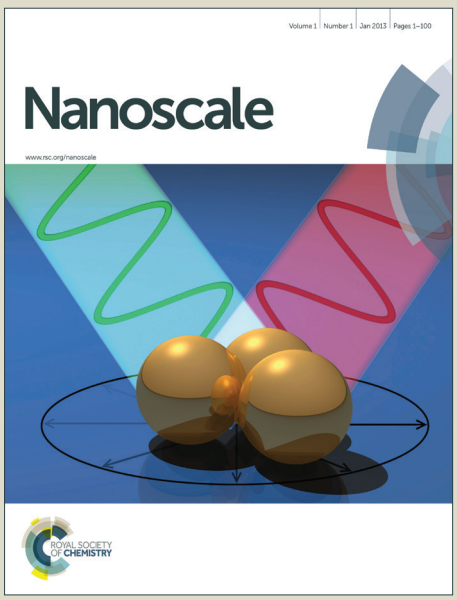

ROYAL SOCIETY OF CHEMISTRY

www.rsc.org/nanoscale

Tuneable paramagnetic susceptibility and exciton g-factor in Mn-doped PbS colloidal nanocrystals

L. Turyanska,[*] R. J. A. Hill, O. Makarovsky, F. Moro, A. N. Knott, O. J. Larkin and A. Patanè[*]

School of Physics and Astronomy, The University of Nottingham, Nottingham NG7 2RD, UK

A. Meaney and P. C. M. Christianen

High Field Magnet Laboratory, Institute for Molecules and Materials, Radboud University, Nijmegen 6525 ED, The Netherlands

M. W. Fay

Nottingham Nanotechnology and Nanoscience Centre, Nottingham NG7 2RD, UK

R. J. Curry

Advanced Technology Institute, Faculty of Engineering and Physical Sciences, University of Surrey, Guildford, GU2 7XH

[*]**Corresponding authors:**

Lyudmila.Turyanska@nottingham.ac.uk, Amalia.Patane@nottingham.ac.uk

KEYWORDS: Magnetic doping, colloidal semiconductor nanocrystals, lead sulfide, exciton g-factor, magnetic susceptibility

ABSTRACT

We report on PbS colloidal nanocrystals that combine within one structure solubility in physiological solvents with near-infrared photoluminescence, and magnetic and optical properties tuneable by the controlled incorporation of magnetic impurities (Mn). We use high magnetic fields (*B* up to 30 T) to measure the magnetization of the nanocrystals in liquid and the strength of the *sp-d* exchange interaction between the exciton and the Mn-ions. With increasing Mn-content from 0.1% to 7%, the mass magnetic susceptibility increases at a rate of ~ 10^{-7} m^3/kg per Mn percentage; correspondingly, the exciton *g*-factor decreases from 0.47 to 0.10. The controlled modification of the paramagnetism, fluorescence and exciton g-factor of the nanocrystals is relevant to the implementation of these paramagnetic semiconductor nanocrystals in quantum technologies ranging from quantum information to magnetic resonance imaging.

Research on low dimensional systems has greatly advanced our understanding of the effects of quantum confinement on fundamental physical properties [1-5]. In particular, recent studies on the incorporation of magnetic impurities in individual zero-dimensional semiconductor nanostructures (quantum dots, QDs) [6-9] has enabled the observation of quantum phenomena of fundamental and technological interest, including Rabi-oscillations [10], and the manipulation of the electron [11-12] and exciton [13-14] spin. These phenomena have potential applications in quantum information processing and are currently investigated both theoretically and experimentally [15-18].

Of key importance in the exploitation of the exciton spin degree of freedom in quantum technologies is the ability to initialize, manipulate and measure the exciton states. This could be achieved, for example, in QDs that have a zero exciton *g*-factor, so that spin-up/spin-down states can be equally populated and controlled by left- and right-circularly polarized light (σ^+ and σ^-). To date, methods for tailoring the excitonic properties have made use of quantum confinement [19-20], externally applied electric fields [21] and doping of the QDs with magnetic impurities [17, 22]. Although these phenomena have been investigated theoretically [15, 23-24] and demonstrated experimentally [13-14, 17, 25], the effects of an increasing incorporation of magnetic impurities on the exciton *g*-factor are still largely unknown. This is partially due to difficulties in controlling and assessing the incorporation of a small concentration of magnetic impurities in the QDs. Also, previous work has focused mainly on epitaxially grown self-assembled QDs [16, 20-21]. Colloidal magnetically doped semiconductor nanocrystals, on the other hand, offer a number of advantages over the latter, including a relatively inexpensive synthesis that is up-scalable, a greater flexibility in tailoring electronic properties by surface chemistry and the use of functional matrices, and solubility in physiological solvents advantageous for bio-medical applications [26].

Here we focus on Mn-doped colloidal PbS QDs. The PbS QDs belong to a class of narrow energy gap IV-VI compounds with band structure and electronic properties that distinguish them from II-VI (CdSe, CdTe, *etc.*) and III-V (InAs, InP, *etc.*) nanostructures. The large Bohr radius of the exciton (ρ = 20 nm) and the small QD diameter (d < 10 nm) make possible a regime of strong confinement of carriers, thus resulting in a quantization energy considerably larger than the energy gap of bulk PbS (E_g = 0.42 eV at T = 290 K) [27]. More importantly, unlike wide band gap II-VI nanocrystals where the Mn-impurity creates an alternative recombination path for carriers [28], in narrow gap IV-VI nanocrystals the photoluminescence (PL) emission from the Mn-dopants is either not observed or else is much weaker than the QD PL emission that occurs at much lower energies [29]. Also, recent theoretical studies [23] have shown that the incorporation of magnetic ions in IV-VI QDs can strongly modify the QD inter-band absorption spectra and electron *g*-factor. Thus this class of nanocrystals and the ability to control their doping and interaction with light and externally applied magnetic fields offer unique opportunities and potential for applications.

In this work, we report on PbS colloidal nanocrystals in water with magnetic and optical properties tailored by the controlled incorporation of Mn-impurities. We use high magnetic fields, B, up to 30T and a combination of structural, magnetic and photoluminescence studies to investigate the effects of Mn-impurities on the electronic and magnetic properties of the nanocrystals. We use high magnetic field gradients to measure directly the QD mass magnetic susceptibility, χ_m, and show that an increasing Mn-content induces a systematic increase of χ_m and a monotonic decrease of the degree of circular polarization (*DCP*) of the QD PL emission. The measured change in the *DCP* corresponds to a decrease of the effective exciton *g*-factor from 0.47 to 0.10 for a Mn content increasing from 0.1% (~2 Mn ions per QD) to 7% (~ 150 Mn ions per QD). We attribute the Mn-induced decrease of the *g*-factor to the *sp-d* exchange interaction

between the exciton and the local magnetic moments of the magnetic ions. We estimate that a critical Mn-doping level of ~ 10% is required to reverse the *g*-factor in PbS QDs with diameter $d \sim 5$ nm. The monotonic decrease of the *g*-factor with increasing Mn-content has been predicted theoretically for lead chalcogenide QDs [23], but never observed experimentally and provides insights into the electronic properties of magnetic colloidal IV-VI nanocrystals relevant for implementations of these QDs in spintronics and quantum technologies. Also, since these paramagnetic fluorescent QDs could find applications as contrast labels in magnetic resonance imaging and multi-modal medical imaging.

RESULTS AND DISCUSSION

For our studies we use colloidal thiol-capped PbS QDs synthesized in aqueous solution with Mn = 0.1%, 1%, 3.5% and 7%. Details of the synthesis are reported elsewhere [29]. Solutions containing the QDs were stored under nitrogen atmosphere at $T = 5$ ºC and were drop-casted on a glass substrate for the optical studies. The Mn-doped PbS quantum dots used in this study have an average diameter $d = 4.5 \pm 1.4$ nm, as derived from atomic force microscopy (AFM) and transmission electron microscopy (TEM) studies, and is independent of the Mn-content (Figure 1a, c). Selected area electron diffraction pattern indicates that the nanocrystals retain the rock-salt crystal structure of bulk PbS. Energy-dispersive X-ray spectroscopy (EDX) experiments were performed on ensembles of nanocrystals to estimate the Mn-content. The EDX spectra (Figure 1b) reveal the characteristic EDX peak associated with Mn at an energy of 5.9 keV. The Mn-concentration, Mn_{EDX}, estimated from the analysis of the EDX data (inset in Figure 1b) is smaller than the nominal Mn-content, *i.e.* only a fraction of Mn used in the precursor solution is incorporated in the nanocrystals. For example, $Mn_{EDX} = 4\%$ for nominal Mn-content 10%, which corresponds to an average number of Mn-ions per QD, $n_{Mn} = 110$. As can be seen in

Figure 1b, the deviation of Mn_{EDX} from the nominal Mn-content increases at high Mn. Correspondingly, the QD PL emission blue-shifts from 1.17 eV to 1.43 eV for Mn increasing from 0.1% to 7% (Figure 2). This is accompanied by an approximately linear shift of the longitudinal optical (LO) phonon Raman peak (see Supplementary information, S1). The weak Mn-related PL band is centred at ≈ 1.9 eV at room temperature, at a higher energy than the much stronger QD PL emission. Since the average diameter and size distribution of the nanocrystals are not changed by Mn, we attribute the energy shift of the QD PL emission and of the LO Raman peak to the inclusion of Mn within the nanocrystals. According to Vegard's law, the band gap energy of a (PbMn)S alloy should increase with increasing Mn and we find that the Mn-concentration, Mn_{PL}, derived from the measured and calculated energy of the QD PL emission is consistent with that derived from the EDX studies (Mn_{EDX}) [29].

The incorporation of Mn-atoms in PbS nanocrystals imparts the nanoparticles with paramagnetic properties, which we probe using EPR (inset in Figure 2) and magnetic susceptibility measurements in strong gradient magnetic field, B_{max} ~ 16 T (Figure 3). The room temperature (T = 300K) EPR spectra reveal six lines superimposed onto a broad signal (inset of Fig. 2 showing the EPR spectra for x = 0.1% and 0.5%). The six line pattern is typical for magnetic resonance transitions between states that are split by the hyperfine interaction between the *d*-shell electrons and the nuclear spins of individual, isolated Mn^{2+} ions in the QDs (states with S = 5/2 and I = 5/2). A broad line is superimposed on the six lines and ascribed to Mn-Mn dipolar broadening and strain of the Hamiltonian parameters. The sextet is centered close to the free electron g_e-value, g = 2.0025, with an isotropic hyperfine constant A ~ 9.3 mT. We do not observe any significant effect of the Mn-content on the position of the EPR peaks. With decreasing Mn-content, the resolution of the six lines in the spectrum improves. However they retain a broadened asymmetric shape, thus suggesting that Mn-ions are incorporated onto

different sites, *i.e.* in the QD core (Mn_{Pb}) and on the surface. This observation is further confirmed by preliminary pulsed-EPR experiments, which can probe weak interactions of Mn-ions close to the surface with hydrogen-atoms on the capping ligands of the nanocrystals, as demonstrated for Mn-doped ZnO nanoparticles [10].

The effect of Mn-doping on the magnetic properties of the QDs is evident from our magnetic susceptibility measurements. This technique allows *direct* measurement of the magnetic susceptibility of colloidal QDs in liquid. For these measurements, a sample container was first filled with de-gassed pure water and suspended in the upper section of the magnet bore where the water, being diamagnetic, was repelled upwards away from the strong magnetic field at the center ($B \sim 16$ T) [30-31]. The current in the superconducting solenoid was increased until the water was effectively weightless (see inset in Figure 3 and Supplementary information, S2). The water was then replaced with the colloidal solution of the QDs. From the measurements of the magnetic force acting on the sample we derived the magnetic susceptibility of the QDs. From this experiment we were not able to measure the magnetic susceptibility of PbS QDs as the associated change of weight was too small to be resolved (bulk PbS is diamagnetic with $\chi_m^{bulk} = -4\times10^{-9}\,\mathrm{m^3/kg}$) [27]. Following the incorporation of Mn, the amplitude and sign of χ_m changes: χ_m becomes positive and its value increases with increasing Mn-content (Figure 3). For QDs with 4.5% Mn, we find that $\chi_m = +(0.42\pm0.03)\times10^{-6}\,\mathrm{m^3/kg}$.

The interaction of the optically excited carriers with the magnetic ions was probed by studies of the degree of circular polarization of the QD PL emission in magnetic field. Figure 4 shows the circularly polarized PL spectra of the Mn-doped PbS QDs at $B = 30$T and $T = 8$K. The PL spectra indicate a systematic decrease in the *DCP* of the QD PL emission with increasing Mn-content. We estimate the *DCP* using the expression $DCP = \left(I_{\sigma^-} - I_{\sigma^+}\right)/\left(I_{\sigma^-} + I_{\sigma^+}\right)$, where I_{σ^+}

and $I_{\sigma-}$ represent the peak intensities of the right and left circular polarized QD PL emission, respectively. For samples with Mn < 1%, the *DCP* increases with increasing magnetic field and tends to saturate at $B > 15$T (Figure 5a). This dependence is similar to that reported previously for our undoped PbS QDs.[32] However, for samples with higher Mn-content, the *DCP* is significantly smaller and tends to saturate at much higher magnetic fields ($B \sim 30$T). At $B = 30$T, the *DCP* decreases from 45% to 18% for a Mn-content increasing from Mn = 0.1% to 7% (Figure 5b). We note that the *DCP* is independent of the excitation power within the studied range ($P = 10$ - 100 W/m^2) and we do not observe any effect of optical heating on the *DCP*, as reported previously for Mn-doped II-VI QDs [24, 33]. Also, *DCP* values are independent of excitation wavelengths in the range 700 - 950 nm.

To explain the systematic decrease of the *DCP* with increasing Mn-content, we analyze the *DCP* data using a simple semiclassical model [34]. The Zeeman interaction of the electron and hole spin with the magnetic field splits the degenerate bright exciton states with total angular momentum $J = 1$. The corresponding Zeeman energy splitting is expressed as $\Delta E_\theta = g_X \mu_B B \cos\theta$, where g_X is the exciton *g*-factor, μ_B is the Bohr magneton constant and θ represents the angle between *B* and the preferential axis of polarization of the nanocrystal. Since the QDs are randomly oriented with respect to the *B*-field, the value of θ is averaged out and the following expression is used to model the *DCP* [34]:

$$DCP = \frac{\int_0^{\pi} 2\cos\theta \tanh(\Delta E / 2k_B T)\sin\theta d\theta}{\int_0^{\pi}(1+\cos^2\theta)\sin\theta d\theta} \frac{1}{1+\tau_s/\tau}. \quad (1)$$

Here τ_s and τ represent the spin relaxation and recombination time of the exciton, respectively. The *DCP* versus *B* curves are fitted to equation (1), see Figure 5a. The least square fits are

obtained with the values of the exciton *g*-factor, g_X, and with the ratio τ_s/τ shown in Figures 5a-b (black-circle data points) for different Mn-concentrations. It can be seen that increasing Mn from 0.1% to 7 % results in a decrease of g_X from 0.47 to 0.10 and a corresponding increase of τ_s/τ from 0.5 to 6.5. The values of g_X derived from the analysis of the *DCP* using equation (1) are in good agreement with those determined from the measured Zeeman energy splitting of the QD PL emission (blue square data points in Figure 6a). Also, the values of τ_s/τ obtained from the fit of the *DCP* using the measured Zeeman splitting at various Mn are in good agreement with those derived using g_X as a fitting parameter.

To account for the contribution to g_X of the *sp-d* exchange interaction between the exciton and the local magnetic moments of the magnetic ions, we use an empirical model in which we express g_X as the sum of two terms $g_X = g + xg_{sp-d}$, where *x* is the Mn-content, *g* is the exciton *g*-factor for $x = 0$ and g_{sp-d} is a constant term that accounts for the contribution of the *sp-d* exchange interaction [13, 15]. From the fit of the experimental values of g_X to this expression (see Figure 6a), we find that $g = 0.39 \pm 0.04$ and $g_{sp-d} = -3.91 \pm 0.92$. Thus with increasing Mn-content, the *sp-d* exchange interaction tends to dominate the intrinsic Zeeman splitting. Our data suggest that a crossover between the σ^+ and σ^- PL emissions of the QDs and a sign reversal of g_X should occur for a Mn-content of ~ 10%.

A monotonic decrease of g_X with increasing Mn was predicted theoretically for diluted magnetic II-VI [15] and IV-VI QDs [23]. In particular, it was shown that the unique energy band structure of IV-VI QDs plays an essential role in the way magnetic ions influence optical transitions with the exchange coupling affecting both the conduction and valence band states. This effect depends on the composition of the crystal (e.g. PbSe, PbTe and PbS), Mn-doping and

QD morphology [23]. Thus different values of g_X could be observed in seemingly similar nanocrystals [14]. A magnetic field dependence of g_X has also been predicted theoretically [15, 23]. From our results we are unable to extract the effect of B on g_X since even at B = 30T the Zeeman splitting is very small (< 1 meV) and cannot be derived accurately from the broad QD PL emission.

Regarding the effects of the Mn-impurities on the ratio τ_s/τ, our independent PL decay studies indicate that the presence of Mn-impurities in the PbS QDs tends to shorten the exciton lifetime τ. The PL lifetime decreases by a factor of ~3 with increasing Mn content from 0% to 5% at all temperatures in the measured range T = 4K to 250K (see Figure S3 in the Supplementary Materials). This decrease is likely to be associated with the presence of Mn-induced carrier traps and could partially account for the systematic increase of the ratio τ_s/τ with increasing Mn shown in Figure 5b. A further contribution to the dependence of τ_s/τ on Mn-content may arise from the Mn-induced increase of the spin-relaxation time previously reported for Mn-doped ZnO QDs [10].

CONCLUSIONS

In summary, we have reported a systematic change of the magnetic and magneto-optical properties of PbS QDs doped with an increasing concentration of Mn-impurities. The large magnetic moments of the impurities impart the QDs with paramagnetic properties and induce a large increase of the magnetic susceptibility. To the best of our knowledge, this is the first report of the direct measurement of the effect of magnetic doping on the magnetic susceptibility of colloidal nanocrystals in liquid. In addition, we found that the *sp-d* exchange interaction between the exciton and the local magnetic ions modifies the exciton *g*-factor. Our data on the degree of

circular polarizarion of the QD PL emission indicate a systematic decrease of the exciton *g*-factor with increasing Mn-content. These results will stimulate further research on the modeling of diluted magnetic IV-VI QDs and their implementation in technologies that exploit the magnetic and exciton properties of these nanocrystals.

EXPERIMENTAL SECTION

Morphological and optical studies. The optical excitation was provided by the 532 nm line of a solid state laser and an excitation power in the range P = 10-100 W/m^2. The luminescence was dispersed by a 150 g/mm grating and detected by either a nitrogen-cooled (InGa)As array photodiode or a charge-coupled device (CCD). For Raman measurements samples were drop-casted on glass or quartz slides. Raman spectra were acquired at T = 300K using laser excitation at λ = 633nm and power density P = 100W/cm^2. For the transmission electron microscopy (TEM) study, the nanocrystals were deposited on a graphene-coated grid, and TEM images were recorded on the JEOL1200EX microscope operating at 120 kV.

Studies in magnetic fields. Room temperature X-band EPR spectra of freeze-dried PbS:Mn samples were recorded on a commercial Bruker E580 spectrometer (Bruker BioSpin GmbH, Rheinstetten, Germany) coupled to a dielectric ring resonator (MD5). The modulation magnetic field amplitude and frequency were 0.1 mT and 100 KHz, respectively.

The magnetic susceptibility was measured in liquid using a custom-built magnetic susceptibility balance with inhomogeneous magnetic field provided by a superconducting magnet (B ~ 16 T). In our experiment a cylindrical plastic sample container with volume of 1 ml was suspended inside the magnet bore by a glass fiber. The fiber was hung from an electronic balance in order to measure the vertical force on the sample, which is the sum of its weight and the magnetic force acting on it. The magnet bore was filled with dry N_2 gas at atmospheric pressure

to displace the oxygen in the air, which, being paramagnetic, gives rise to undesirable thermomagnetic convection within the bore and can contaminate the liquid sample. The sample container was filled with de-gassed pure water and suspended in the upper section of the bore.

For the PL studies in magnetic fields up to 30T, the samples were mounted on an optical probe and cooled inside a liquid helium bath cryostat in a 33T Bitter-type electromagnet. Two circular polarizations, σ^+ and σ^-, of the QD PL emission were measured in Faraday configuration using a circular polarizer ($\lambda/4$ and linear polarizer) over two successive sweeps of magnetic field with opposite directions.

Author contribution. LT and AP have designed the research study. LT has performed and/or participated in all experiments and synthesized the nanocrystals. Other co-authors contributed to the magnetic susceptibility study (RJAH and OJL); photoluminescence in high magnetic fields (AM and PCMC); theoretical modelling (OM); EPR spectroscopy (FM); Raman studies (ANK), structural characterization (MWF); and time resolved photoluminescence measurements (RJC). All authors have contributed to writing the manuscript.

Acknowledgements. This work is supported by The University of Nottingham and The Leverhulme Trust. We acknowledge the support of the HFML-RU/FOM, member of the European Magnetic Field Laboratory (EMFL, EuroMagNET II) under the EU contract number 228043 and the Photon Science Institute and the EPSRC multi-frequency EPR national facility at the University of Manchester. The authors acknowledge Prof. Neil R. Thomas for useful discussions and for enabling access to the chemistry laboratory in the School of Chemistry at Nottingham. RJAH acknowledges support from an EPSRC Fellowship, grant number EP/I004599/1.

Supporting Information Available: Details of the experiments techniques and results are available for the following studies: Raman and PL lifetime measurements, and magnetic susceptibility investigation.

REFERENCES

[1] Rogach A. L. (ed), Semiconductor nanocrystal quantum dots. Springer Wien New York **2010**, ISBN 978-3-211-99913-4.

[2] Scholes G. D.; and Rumbles G. Excitons In Nanoscale Systems. *Nat. Mater.* 2006, **5**, 683.

[3] Kim J. Y.; Voznyy O.; Zhitomirsky D.; Sargent E. H. 25th Anniversary Article: Colloidal Quantum Dot Materials And Devices: A Quarter-Century of Advances. *Adv. Mater.* 2013, **25**, 4986.

[4] Wolf S. A.; Awschalom D. D.; Buhrman R. A.; Daughton J. M.; von Molnar S.; Roukes M. L.; Chtchelkanova A. Y.; Treger D. M. Spintronics: A Spin-Based Electronics Vision For The Future. *Science* 2001, **294**, 1488.

[5] Babinski A.; Potemski M.; Christianen P. C. M. Optical Spectroscopy On Semiconductor Quantum Dots In High Magnetic Fields. *C. R. Physique* 2013, **14**, 121.

[6] Buonsanti R.; Milliron D. J. Chemistry of Doped Colloidal Nanocrystals. *Chemistry of Materials* 2013, **25**, 1305.

[7] Mocatta D.; Cohen G.; Schattner J.; Millo O.; Rabani E.; Banin U. Heavily Doped Semiconductor Nanocrystal Quantum Dots. *Science* 2011, **332**, 77.

[8] Freitas Neto E. S.; Dantas N. O.; Lourenco S. A.; Teodoro M. D.; Marques G. E. Magneto-Optical Properties of $Cd_{1-x}Mn_xS$ Nanoparticles: Influences of Magnetic Doping, Mn^{2+} Ions Localization, And Quantum Confinement. *Phys. Chem. Chem. Phys.* 2012, **14**, 3248.

[9] Yang B.; Shen X.; Zhang H.; Cui Y.; Zhang J. Luminescent and Magnetic Properties in Semiconductor Nanocrystals With Radial-Position-Controlled Mn^{2+} Doping. *J. Phys. Chem. C* 2013, **117**, 15829.

[10] Ochsenbein S. T.; Gamelin D. R. Quantum Oscillations in Magnetically Doped Colloidal Nanocrystals. *Nat. Nanotech.* 2011, **6**, 112.

[11] Grumbach N.; Rubin-Brusilovski A.; Maikov G. I.; Tilchin E.; Lifshitz E. Manipulation Of Carrier-Mn^{2+} Exchange Interaction in CdTe/CdSe Colloidal Quantum Dots by Controlled Positioning of Mn^{2+} Impurities. *J. Phys. Chem. C* 2013, **117**, 21021.

[12] Morley G. W.; Lueders P.; Mohammady M. H.; Balian S. J.; Aeppli G.; Kay C. W. M.; Witzel W. M.; Jeschke G.; Monteiro T. S. Quantum Control of Hybrid Nuclear-Electronic Qubits. *Nat. Mater.* 2013, **12**, 103.

[13] Schmidt T.; Scheibner M.; Worschech L.; Forchel A.; Slobodskyy T.; Molenkamp L. W. Sign Reversal and Light Controlled Tuning of Circular Polarization in Semimagnetic CdMnSe Quantum Dots. *J. Appl. Phys.* 2006, **100**, 123109.

[14] Long G.; Barman B.; Delikanli S.; Tsai Y. T.; Zhang P.; Petrou A.; Zang H. Carrier-Dopant Exchange Interactions In Mn-Doped PbS Colloidal Quantum Dots. *Appl. Phys. Lett.* 2012, **101**, 062410.

[15] Chang K.; Xia J. B.; Peeters F. M. Magnetic Field Tuning Of The Effective g-Factor in a Diluted Magnetic Semiconductor Quantum Dot. *Appl. Phys. Lett.* 2003, **82**, 2661.

[16] Takahashi S.; Deacon R. S.; Oiwa A.; Hirakawa K.; Tarucha S. Electrically Tunable Three-Dimensional g-Factor Anisotropy in Single InAs Self-Assembled Quantum Dots. *Phys. Rev. B* 2013, **87**, 161302(R).

[17] Bussian D. A.; Crooker S. A.; Yin M.; Brynda M.; Efros A. L.; Klimov V. I. Tunable Magnetic Exchange Interactions in Manganese-Doped Inverted Core–Shell ZnSe–CdSe Nanocrystals. *Nat. Mater.* 2009, **8**, 35.

[18] Viswanatha R.; Pietryga J.; Klimov V. I.; Crooker S. A. Spin-Polarized Mn^{2+} Emission from Mn-Doped Colloidal Nanocrystals. *Phys. Rev. Lett*. 2011, **107**, 067402.

[19] Zhu Y.-H.; Xia J.-B. Controllable Electron g-Factors in HgMnTe Quantum Spheres. *EPL* 2008, **82**, 37004.

[20] Kleemans N. A. J. M.; van Bree J.; Bozkurt M.; van Veldhoven P. J.; Nouwens P. A.; Nötzel R.; Silov A. Yu.; Koenraad P. M.; Flatte M. E. Size-Dependent Exciton g-Factor in Self-Assembled InAs/InP Quantum Dots. *Phys. Rev. B* 2009, **79**, 045311.

[21] Klotz F.; Jovanov V.; Kierig J.; Clark E. C.; Rudolph D.; Heiss D.; Bichler M.; Abstreiter G.; Brandt M. S.; Finley J. J. Observation of an Electrically Tunable Exciton g-Factor in InGaAs/GaAs Quantum Dots. *Appl. Phys. Lett.* 2010, **96**, 053113.

[22] Pacuski W.; Ferrand D.; Cibert J.; Deparis C.; Gaj J. A.; Kossacki P.; Morhain C. Effect of the s ,p-d Exchange Interaction on the Excitons in $Zn_{1-x}Co_xO$ Epilayers. *Phys. Rev. B* 2006, **73**, 035214.

[23] Prado S. J.; Villegas-Lelovsky L.; Alcalde A. M.; Lopez-Richard V.; Marques G. E. Magneto-Optical Properties in IV-VI Lead-Salt Semimagnetic Nanocrystals. *Nanoscale Research Letters* 2012, **7**, 374.

[24] Kłopotowski Ł.; Cywi´nski Ł.; Szymura M.; Voliotis V.; Grousson R.; Wojnar P.; Fronc K.; Kazimierczuk T.; Golnik A.; Karczewski G.; Wojtowicz T. Influence of Exciton Spin Relaxation on the Photoluminescence Spectra of Semimagnetic Quantum Dots. *Phys. Rev. B* 2013, **87**, 245316.

[25] Norris D. J.; Yao N.; Chamock F. T.; Kennedy T. A. High-Quality Manganese-Doped ZnSe Nanocrystals. *Nano Lett*. 2001, **1**, 3.

[26] Kairdolf B. A.; Smith A. M.; Stokes T. H.; Wang M. D.; Young A. N.; Nie S. Semiconductor Quantum Dots for Bioimaging and Biodiagnostic Applications. *Annu. Rev. Anal. Chem.* 2013, **6**, 143.

[27] The Landolt-Bornstein database. http://www.springermaterials.com/docs/index.html Springer Materials, 2013.

[28] Warad H. C.; Ghosh S. C.; Hemtanon B.; Thanachayanont C.; Dutta J. Luminescent Nanoparticles of Mn Doped ZnS Passivated with Sodium Hexametaphosphate. *Sci. Technol. Adv. Mater.* 2005, **6**, 296.

[29] Turyanska L.; Moro F.; Knott A. N.; Fay M. W.; Bradshaw T. D.; Patanè A. Paramagnetic, Near-Infrared Fluorescent Mn-Doped PbS Colloidal Nanocrystals. *Part. Part. Syst. Charact.* 2013, **30**, 945.

[30] Beaugnon E.; Tournier R. Levitation of Water and Organic Substances in Static High Magnetic Fields. *J. Phys. III France 1* 1991, 1423.

[31] Hill R. J. A.; Eaves L. Vibrations of a Diamagnetically Levitated Water Droplet. *Phys. Rev. E* 2010, **81**, 056312.

[32] Turyanska L.; Blokland J. H.; Elfurawi U.; Makarovsky O.; Christianen P. C. M.; Patanè A. Photoluminescence of PbS Nanocrystals at High Magnetic Fields up to 30T. *Phys. Rev. B* 2010, **82**, 193302.

[33] Jang Y. D.; Badcock T. J.; Mowbray D. J.; Skolnick M. S.; Park J.; Lee D.; Liu H. Y.; Hopkinson M.; Hogg R. A.; Andreev A. D. Enhanced Nonradiative Auger Recombination in p - Type Modulation Doped InAs/GaAs Quantum Dots. *Appl. Phys. Lett.* 2008, **93**, 101903.

[34] Langof L.; Fradkin L.; Ehrenfreund E.; Lifshitz E.; Micic O. I.; Nozik A. J. *Chem. Phys.* 2004, **297**, 93.

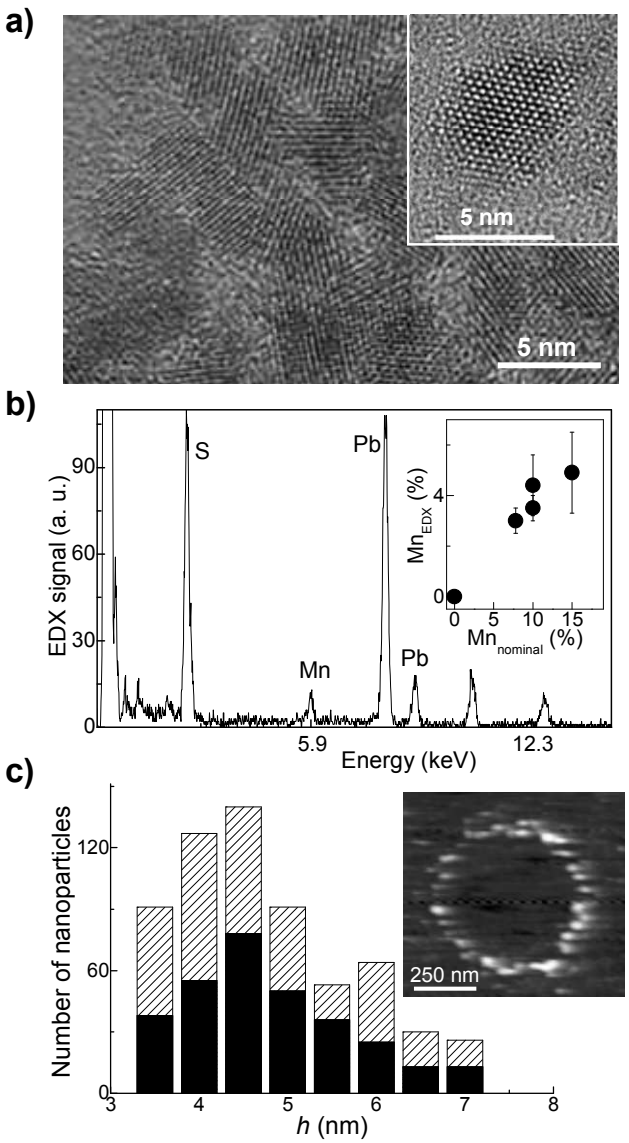

Figure 1. a) High resolution TEM image of Mn-doped PbS QDs with Mn-content of 5%. **b)** EDX spectrum of an ensemble of QDs revealing the characteristic Mn-peak at 5.9 keV and (inset) Mn-content in the QDs as estimated from EDX (Mn_{EDX}) versus the nominal Mn-content used in the synthesis. The error in the Mn-doping level is estimated from multiple EDX measurements. **c)** Histogram showing the size distribution of the QDs as derived from AFM for PbS QDs with $Mn_{EDX} = 0\%$ (black bars) and 5% (patterned bars). Inset: AFM image of Mn-doped PbS QDs.

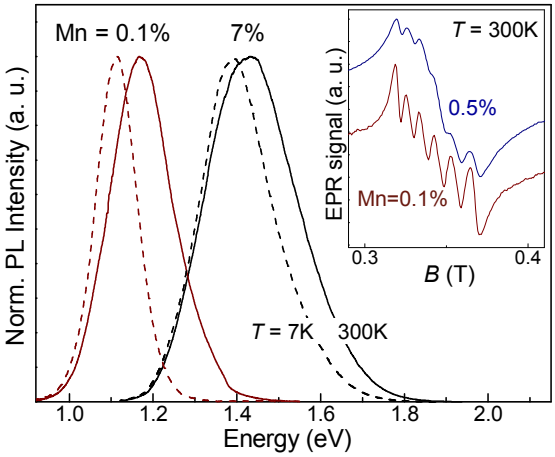

Figure 2. Photoluminescence (PL) spectra of PbS:Mn QD ensembles at T = 300K (continuous line) and at T = 7K (dashed line). Inset: Room temperature X-band EPR spectra of Mn-doped PbS QDs with 0.1% and 0.5% of Mn.

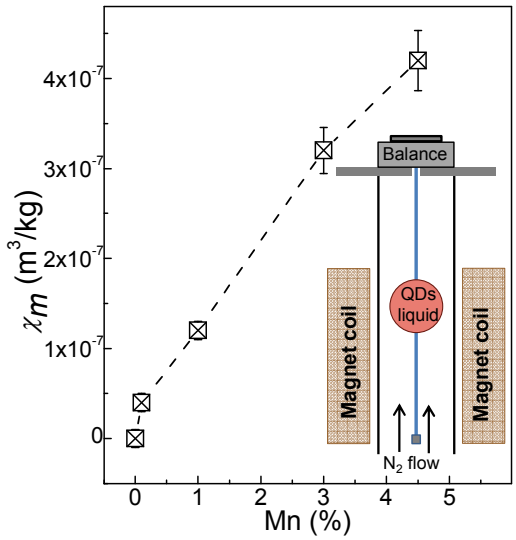

Figure 3. Mass magnetic susceptibility, χ_m, of Mn-doped PbS QDs as a function of the Mn-content at T = 300K and B_{max} = 16T. The inset shows a sketch of the experimental set-up used to measure χ_m. In this experiment a cylindrical plastic sample container with volume of 1 ml was suspended inside the magnet bore by a glass fiber. The fiber was hung from an electronic balance in order to measure the vertical force on the sample, which is the sum of its weight and the magnetic force acting on it. The magnet bore was filled with dry N_2 gas at atmospheric pressure to displace the oxygen in the air.

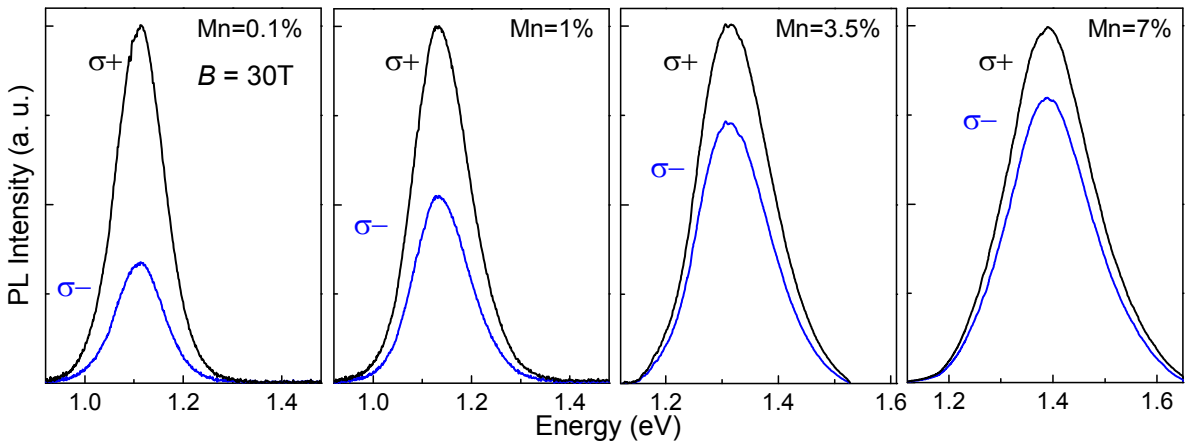

Figure 4. Polarised (σ+ and σ-) PL spectra for PbS:Mn QDs with different Mn-content at B = 30T and T = 7K. For clarity, the PL spectra are normalised to the peak intensity of the σ+ PL spectrum.

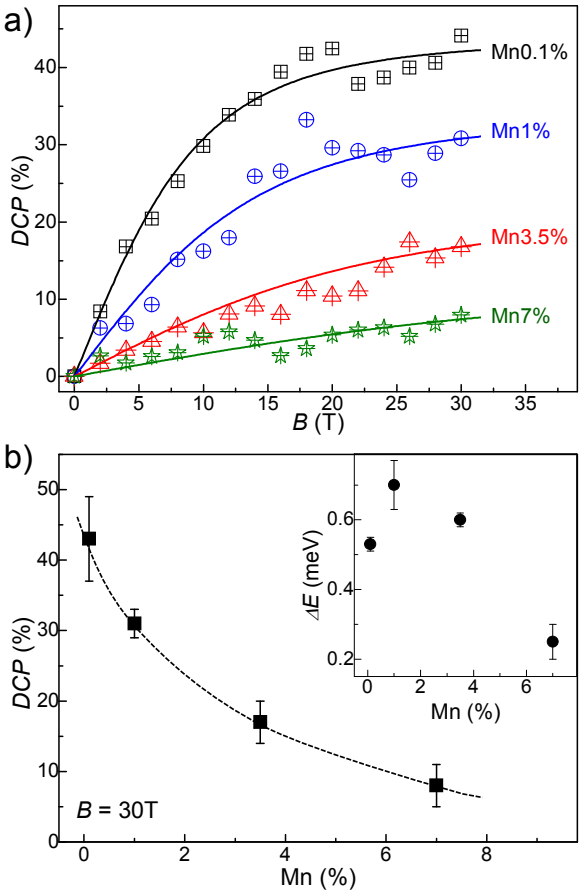

Figure 5. a) Degree of circular polarization (*DCP*) data at T = 7K averaged over 4 repeats. Curves are fitted by the method of least squares with two free fitting parameters: τ_s/τ and g_X. **b)** Dependence of the *DCP* on Mn-content and (inset) Zeeman splitting, ΔE, at B = 30T and T = 7K. Error bars represent a standard deviation of 4 measurements.

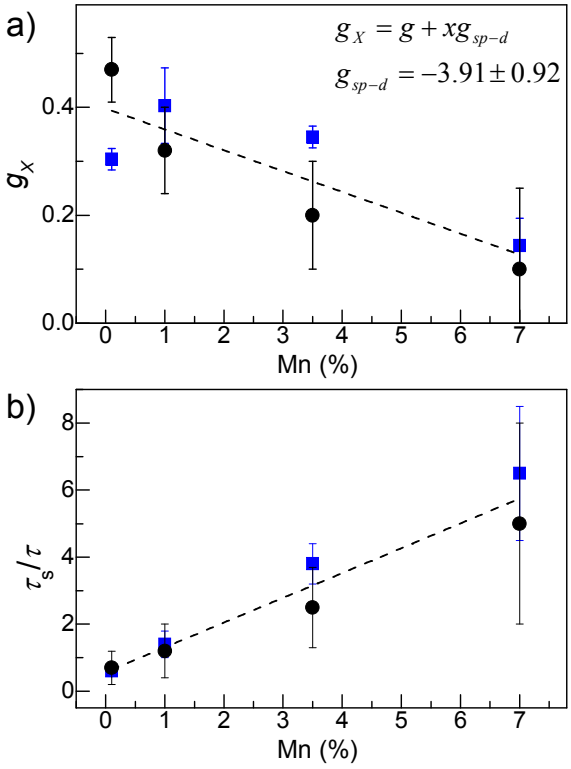

Figure 6. a) Exciton g-factor, g_X, and **b)** τ_s/τ as derived from fitting the *B*-dependence of the *DCP* (black circles) and as estimated from the Zeeman splitting (blue squares). For fitted data points, error bars represent error of the fit. For data points estimated from the Zeeman splitting, error bars represent a standard deviation of 4 measurements. Dashed lines are guides to the eye.